fractal and fractional

MDPI

Article

A Compact Triple-Band UWB Inverted Triangular Antenna with Dual-Notch Band Characteristics Using SSRR Metamaterial Structure for Use in Next-Generation Wireless Systems

Arshad Karimbu Vallappil [1,*], Bilal A. Khawaja [1,*], Mohamad Kamal A. Rahim [2], Muhammad Naeem Iqbal [2], Hassan T. Chattha [3] and Mohamad Fakrie bin Mohamad Ali [2]

[1] Department of Electrical Engineering, Faculty of Engineering, Islamic University of Madinah, P.O. Box 170, Madinah 41411, Saudi Arabia
[2] Advance RF and Microwave Research Group (ARFMRG), School of Electrical Engineering, Faculty of Engineering, Universiti Teknologi Malaysia, UTM Johor Bahru, Johor Bahru 81310, Malaysia; mdkamal@utm.my (M.K.A.R.); naeem.iqbal@graduate.utm.my (M.N.I.); mohamadfakrie@graduate.utm.my (M.F.b.M.A.)
[3] Advanced Cyclotron Systems Inc. (ACSI), Richmond, BC V6X 1X5, Canada; htariq@advancedcyclotron.com
* Correspondence: arshadkv@iu.edu.sa (A.K.V.); 7166@iu.edu.sa (B.A.K.)

Abstract: A compact triple-band operation ultra-wideband (UWB) antenna with dual-notch band characteristics is presented in this paper. By inserting three metamaterial (MTM) square split-ring resonators (MTM-SSRRs) and a triangular slot on the radiating patch, the antenna develops measured dual-band rejection at 4.17–5.33 GHz and 6.5–8.9 GHz in the UWB frequency range (3–12 GHz). The proposed antenna offers three frequency bands of operation in the UWB range, which are between 3–4.17 GHz (~1.2 GHz bandwidth), 5.33–6.5 GHz (~1.17 GHz bandwidth), and 8.9–12 GHz (~3.1 GHz bandwidth), respectively. The higher resonating frequency band can be tuned/controlled by varying the width of the triangle slot, while the medium operational band can be controlled by adjusting the width of the SSRR slot. Initially, the simulated S-parameter response, 2D and 3D radiation patterns, gain, and surface current distribution of the proposed UWB inverted triangular antenna has been studied using epoxy glass FR4 substrate having parameters ε_r = 4.3, h = 1.6 mm, and tan δ = 0.025, respectively. In order to validate the simulation results, the proposed UWB antenna with dual-notch band characteristics is finally fabricated and measured. The fabricated antenna's return-loss and far-field measurements show good agreement with the simulated results. The proposed antenna achieved the measured gain of 2.3 dBi, 4.9 dBi, and 5.2 dBi at 3.5 GHz, 6.1 GHz, and 9.25 GHz, respectively. Additionally, an in-depth comparative study is performed to analyze the performance of the proposed antenna with existing designs available in the literature. The results show that the proposed antenna is an excellent candidate for fifth-generation (5G) mobile base-stations, next-generation WiFi-6E indoor distributed antenna systems (IDAS), as well as C-band and X-band applications.

Keywords: ultra-wideband (UWB); metamaterial (MTM); square split-ring resonator (SSRR); fifth-generation (5G); WiFi-6E; indoor distributed antenna systems (IDAS); C-band; X-band

Citation: Vallappil, A.K.; Khawaja, B.A.; Rahim, M.K.A.; Iqbal, M.N.; Chattha, H.T.; Ali, M.F.b.M. A Compact Triple-Band UWB Inverted Triangular Antenna with Dual-Notch Band Characteristics Using SSRR Metamaterial Structure for Use in Next-Generation Wireless Systems. *Fractal Fract.* **2022**, *6*, 422. https://doi.org/10.3390/fractalfract6080422

Academic Editor: Francesco De Nicola

Received: 27 June 2022
Accepted: 28 July 2022
Published: 30 July 2022

1. Introduction

The proliferation of smart wearable and handheld wireless devices is changing the world as we know it at a fast pace. Our dependency on these wireless devices is due to the availability of high-speed wireless communication systems. It is estimated that approximately 23 billion internet-connected wireless devices are currently used by end-users and this will increase to 100 billion devices by the time the forthcoming fifth-generation (5G) wireless technology is completely deployed, which covers both sub-6 GHz and millimeter-wave frequency bands [1–4]. In addition to this, the use of bandwidth-hungry applications like virtual and augmented reality platforms, online gaming, always-connected social

media platforms, artificial intelligence (AI) applications, and live streaming websites will bring a 1000-fold upsurge in the network capacity which cannot be fulfilled by the currently deployed wireless technologies [1,2]. It is anticipated that currently deployed 5G wireless technology can handle this demand because it offers massive low signal latency and power consumption, and increased bandwidth with data-transmission speeds comparable to an optical fiber by offering ~10 GB/s data rates, and several billion-user connection capacity [4]. Although the researchers and technology companies have already started exploring the possibilities for next-generation wireless technologies such as Beyond 5G (B5G) and sixth-generation (6G) wireless systems as well as broadband Wi-Fi technologies above 6 GHz frequency band such as WiFi-6E [1–4].

In modern and upcoming wireless systems, the most important component in the radio frequency (RF) transceivers is the antenna, which plays a critical part in the way the signal is transmitted to the end-user. Antennas have been assigned functions such as beam-steering/beam-scanning [5,6], multi-band operation [7–9], reconfigurability [10], band-notch characteristics [11–13], and gain-filtering [14]. Moreover, the need for antennas that can operate in multiple frequency bands has exponentially increased in recent years because of the introduction of new and different variants of Wi-Fi standards [2–4]. For example, IEEE 802.11ac Wi-Fi standard offers 5 GHz single-band operation, whereas IEEE 802.11ax (WiFi-6) offers 2.4 GHz/5 GHz dual-band operation, and future standards like WiFi-6E, which will be deployed in the years to come, will offer 2.4 GHz/5 GHz and 6 GHz triple-band operation with ultra-wide bandwidth [2–4,15]. Modern 5G antenna systems are required to have ultra-wideband (UWB) behavior with multi-band coverage and operation to adapt quickly to the newly released standards and their frequency bands [16,17]. This allows for an easy transition to the new wireless standards for the end-users with enhanced data rates, and more bandwidth. It also allows for maintaining the sustainability and competitiveness of wireless communication systems.

UWB antennas are preferred for such systems because of their huge bandwidth characteristics. The Federal Communication Commission (FCC), USA [18] has designated a frequency spectrum ranging from 3.1–10.6 GHz (7.5 GHz bandwidth) for UWB antennas for low-power emission applications. For modern wireless communication systems, microstrip patch antennas (MPAs) [19] are typically preferred and have gained popularity due to their small size and weight, low-cost, ease of fabrication, and compatibility with other transceiver components. The MPAs are also sometimes referred to as planar antennas [19]. The MPAs have some inherent disadvantages: they offer narrow bandwidth, and they typically resonate at a single frequency, although these shortcomings can be overcome by adding slots [7,11,20] and slits [9,12] in the main resonating patch. The UWB antenna can be realized using several techniques. For example, researchers have designed UWB antennas using (1) planar wideband antenna technique, (2) fractal structure oriented UWB antenna technique, (3) MTM inspired UWB antenna technique, and (4) wearable UWB antenna techniques using planar antenna concepts [11–13,17,18,21–26].

One of the serious constraints in the design and operation of UWB antennas is the interference with other neighboring communication systems that use the frequency bands within the UWB range. It is therefore critically important for the researchers and the systems designers to reject or filter these interfering bands, which leads to the concept of filtering, and notch-band characteristics [18]. A number of researchers have proposed and investigated different UWB filter designs with band-rejection capabilities and selectivity at different frequency bands to solve this problem [27]. On the other hand, antennas with band-rejection characteristics can also be designed using different techniques to select certain frequency bands and reject others. This behavior in antennas is also referred to as notch-band characteristics and it can be realized by using techniques like (1) introduction of slots in the resonating patch, and (2) introduction of MTM-oriented structures such as electromagnetic bandgap (EBG) structures, split-ring resonator (SRR) structures, parasitic elements, frequency selective surfaces (FSS)/meta-surfaces, meander-line structures, etc. in the resonating patch [11–13,18,26,28–33]. Depending on the technique employed, the

antenna can be made to reject single as well as multiple frequency bands. In some cases, both the slot- as well as MTM-based techniques can be exploited together to implement effective and useful notch-band characteristics. Most of the researchers had faced difficulties in controlling each operational and rejection band individually.

Therefore, in this paper, the authors exploit both MTM and slot-based techniques and propose a MTM square split-ring resonator (SSRR) structure inspired triple-band operation UWB inverted triangular antenna with dual-notch band characteristics for the currently deployed 5G mobile base-stations (BSs), upcoming WiFi-6E indoor distributed antenna systems (IDAS), as well as C-band and X-band applications, respectively. The antenna operates in the frequency range of the 3–12 GHz band. The radiating patch of the antenna is based on the inverted modified triangular patch. The dual-notch band characteristic of the antenna is achieved by introducing three MTM-SSRRs and a triangular slot in the middle of the patch, which allows measured dual-band rejection at 4.17–5.33 GHz and 6.5–8.9 GHz and operational bands at 3–4.17 GHz, 5.33–6.5 GHz and 8.9–12 GHz. The middle operational band can be controlled by varying the width of the SSRR slot and the higher operational band can be controlled by changing the triangular slot width. The proposed antenna is designed using a flame-resistant (FR4) epoxy glass substrate having substrate thickness (h) of 1.6 mm, dielectric permittivity (ε_r) of 4.3, and loss-tangent ($tan\ \delta$) of 0.025, respectively. The MTM-SSRR antenna offers a compact structure, having overall dimensions of 28 mm $\times$ 40 mm. The proposed antenna exhibits enhanced gain characteristics at higher frequency bands. The rest of the structure of the paper is as follows: Section 2 covers the in-depth study of the antenna design model, the effect of MTM-SSRR analysis on the antenna performance, step-by-step antenna design, and its simulated results. Section 3 discusses the parametric analysis performed during the antenna design stage. The UWB antenna prototyping/measurement setup, simulated/measured parameter responses, E- and H-plane radiation patterns, and antenna gain characteristics are discussed in Section 4. In Section 5, the comparison between the proposed UWB antenna with the existing research literature is performed and the results are summarized. Finally, Section 6 draws conclusions.

2. Antenna Configuration

2.1. Antenna Model

The proposed triple-band UWB antenna with dual-notch band characteristics is shown in Figure 1a–c. Basically, the antenna consists of an inverted triangular radiating patch with a triangular slot in the middle, a 50 Ω microstrip feeding mechanism, a rectangular partial ground plane on the back side of the substrate, and three SSRRs with stub embedded in the radiating patch.

A triangular slot and 3-SSRR with stub embedded in the radiation patch allow for triple-band operation with dual-band rejection. The range of dual-band rejection can be varied by adjusting the dimensions of the slot and SSRRs. The proposed dual-notch band UWB antenna is designed on an FR4 substrate having a thickness (h) of 1.6 mm and dielectric constant (ε_r) of 4.3 with a loss-tangent of 0.025, respectively. The overall size of the proposed antenna is 28 mm $\times$ 40 mm. The antenna parameters are designed and analyzed using the CST Microwave Studio (CST-MWS). Table 1 shows the proposed antenna dimensions.

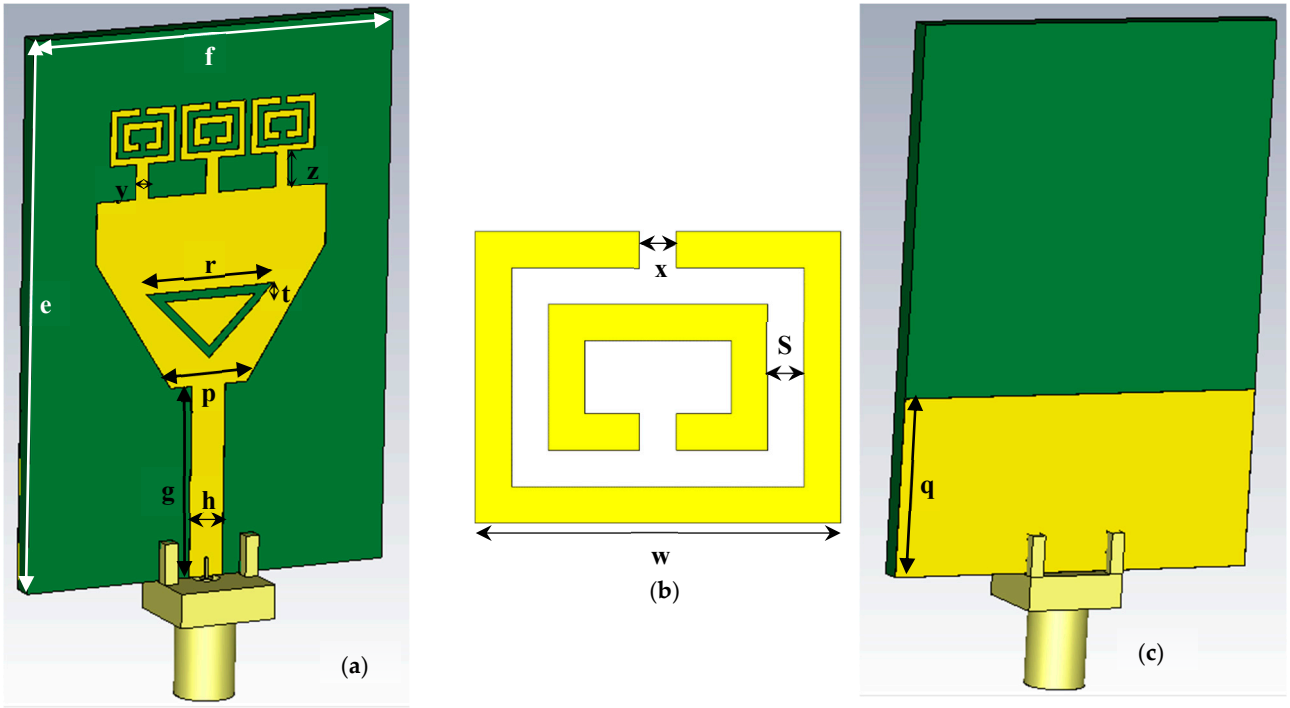

Figure 1. Proposed triple band UWB antenna with dual notch (**a**) Top-layer (**b**) SSRR Unit-cell (**c**) Bottom-layer.

Table 1. Proposed antenna dimensions.

Parameter	Dimension (mm)
E	40 mm
F	28 mm
G	14 mm
H	2.6 mm
W	5 mm
S	0.5 mm
X	0.5 mm
Y	1 mm
Z	2.5 mm
P	6 mm
R	11 mm
T	0.9 mm
Q	13 mm

2.2. SSRR Analysis

The behavior of the material or unit-cell with negative permittivity (ε) and permeability (μ) simultaneously in certain frequency ranges is called metamaterial (MTM). In 1967, Veselago investigated left-handed MTMs (LHMs) and their properties [34]. The refractive index of the medium is measured as being negative due to negative μ and negative ε. In this section, we have discussed the S-parameter response and refractive index of the SSRR unit-cell.

The SSRR unit-cell is printed on an FR4 substrate (h = 1.6 mm, ε_r = 4.3, $tan\ \delta$ = 0.025) to analyze its performance. The unit-cell design and analysis were carried out using CST-MWS. For this design, it can be observed from Figure 2 that the perfect boundary conditions (PBCs) are used on the unit-cell that comprises of only one SSRR, having two sides (along the y-axis) as a perfect electric conductor (PEC), and the other two (along the z-axis) as a perfect magnetic conductor (PMC). For the wave ports, the other two sides of the unit-cell (along the x-axis) are used for excitation and radiation purposes as highlighted in Figure 2.

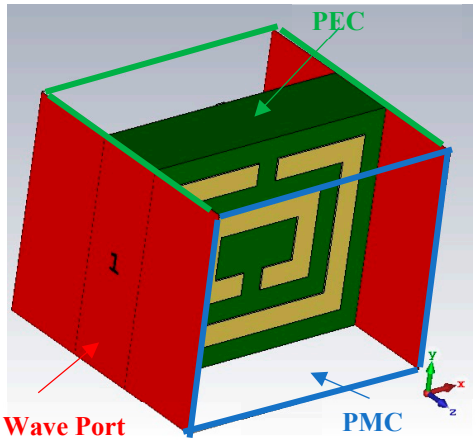

Figure 2. Perfect boundary condition and excitation applied to single unit-cell using CST-MWS.

The S_{11} and S_{12} behavior of the SSRR unit-cell is illustrated in Figure 3a. The unit-cell is resonating between the frequency range of 5.45–7.4 GHz with a return-loss below -10dB. This unit-cell is inserted into the proposed antenna to develop an operational band at 5.45–6.77 GHz and a rejection band at 4.2–5.45 GHz, respectively. These S-parameter values have been used to plot the graph of refractive index (n). The n of the SSRR unit-cell is depicted in Figure 3b. From Figure 3b, it has been observed that the unit-cell has a negative n between the frequency range of 4.2–5.45 GHz. This result reflects that the proposed SSRR unit-cell shows MTM properties and helps to provide a notch-band between the above frequency range by inserting it to the radiating patch of the proposed antenna.

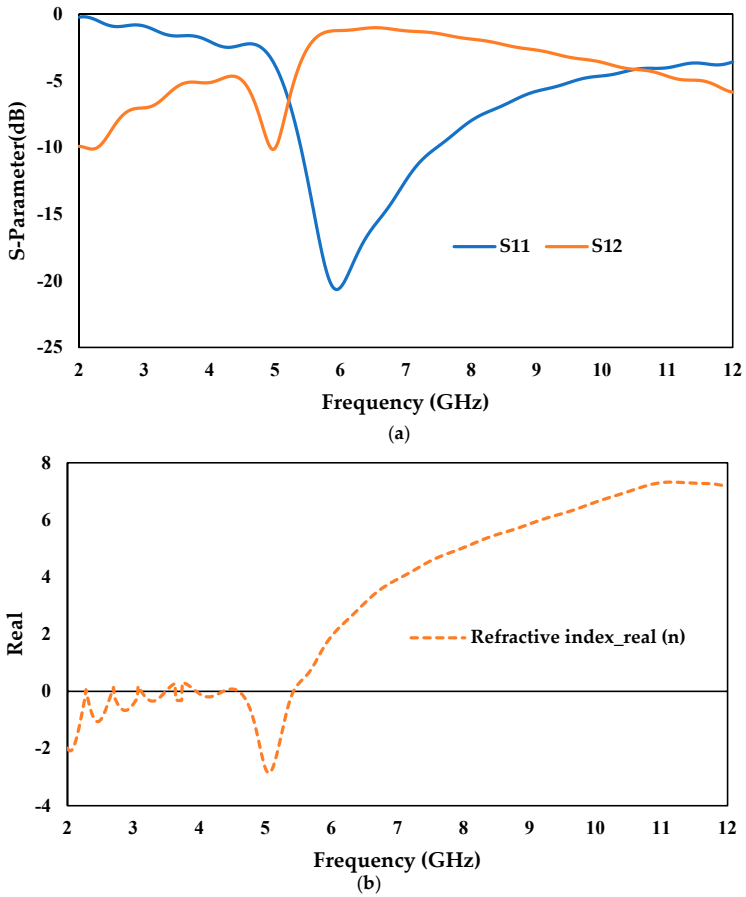

Figure 3. Performance analysis of SSRR unit-cell (**a**) S-parameter response (**b**) Refractive index response.

2.3. Antenna Analysis

Figure 4 shows the step-by-step design of the triple-band UWB antenna with dual-notch band characteristics. Figure 5 shows a performance comparison for the steps involved in the dual-notch band UWB antenna using a reflection coefficient (S_{11}) plot. Table 2 compares the coverage of operational and rejected bands at every step involved in the design. Figure 5 and Table 2 show how different design steps for the proposed UWB antenna influenced the operational and rejection bands coverage. In step-1, the inverted triangular patch antenna with a partial ground plane is operating between 3.4–12 GHz. In step-2, the triangular slot on the radiating patch contributed to achieving dual-band operation with one rejection band between 5.7–8.3 GHz. In the final step, the insertion of 3-SSRRs with stub helps to achieve triple-band operation with two rejection bands between 4.2–5.45 GHz and 6.77–8.7 GHz, respectively.

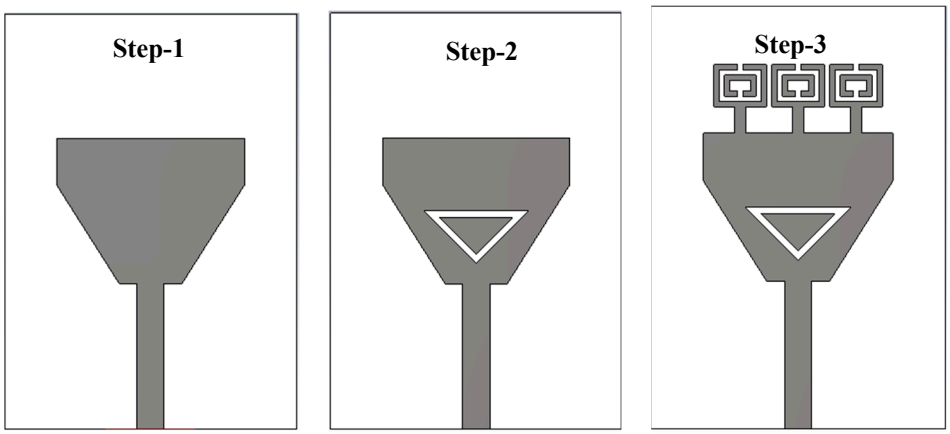

Figure 4. Step-by-Step design of proposed antenna.

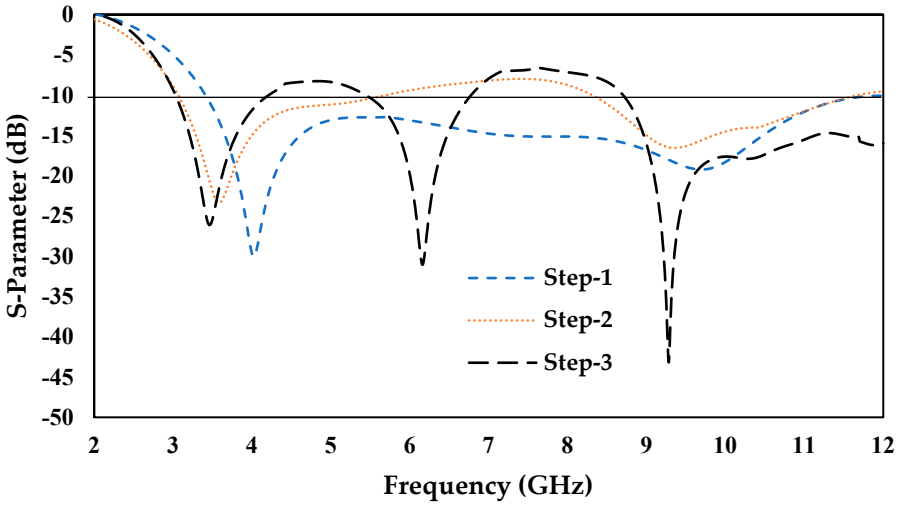

Figure 5. S-Parameter (S_{11}) performance at each design step of proposed antenna.

Table 2. Operational and Rejection band coverage at each design step.

Step No.	No of Operational Bands	Operational Bands Coverage (GHz)	No. of Rejection Bands	Rejection Bands Coverage (GHz)
1	1	3–12	-	-
2	2	3–5.7, 8.3–12	1	5.7–8.3
3	3	3–4.2, 5.45–6.77, 8.7–12	2	4.2–5.45, 6.77–8.7

2.4. Simulated Analysis

The simulated performance of the proposed antenna is presented with the help of the reflection coefficient curve, surface-current distribution, and the 3D radiation patterns (RPs). The proposed triple-band UWB antenna with a dual-notch band characteristics reflection coefficient curve is illustrated in Figure 6. From Figure 6, it was understood that the proposed dual-notch band antenna has three operational frequency bands centered at 3.5 GHz, 6.1 GHz, and 9.25 GHz with a return-loss of −26 dB, −31 dB, and −43 dB, respectively.

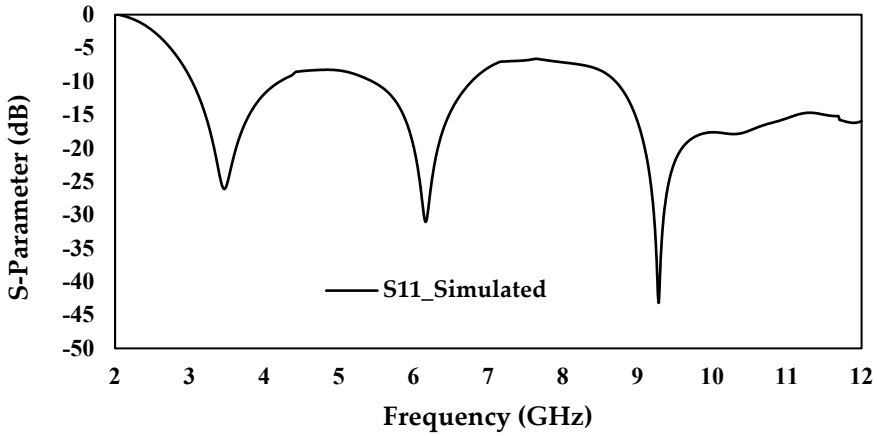

Figure 6. Simulated reflection coefficient curve of the proposed triple-band UWB antenna with dual-notch.

The surface current distributions at 3.5 GHz, 6.1 GHz, and 9.25 GHz are shown in Figure 7a–c. From the graphs, it can be understood that the surface current at 3.5 GHz is greater across the microstrip feed-line and along the edges of the inverted triangular patch. At 6.1 GHz, the surface current distribution is strong at SSRR and edges of the radiating patch. Similarly, at 9.25 GHz, the surface current distribution is stronger at the triangular slot in the middle of the radiating patch. The 3D RPs for the same resonant frequencies are also shown in Figure 8a–c. From the 3D RP plots, it can be observed that the proposed triple-band UWB antenna has peak gains of 2.95 dBi, 5.23 dBi, and 6.2 dBi, at 3.5 GHz, 6.1 GHz, and 9.25 GHz, respectively.

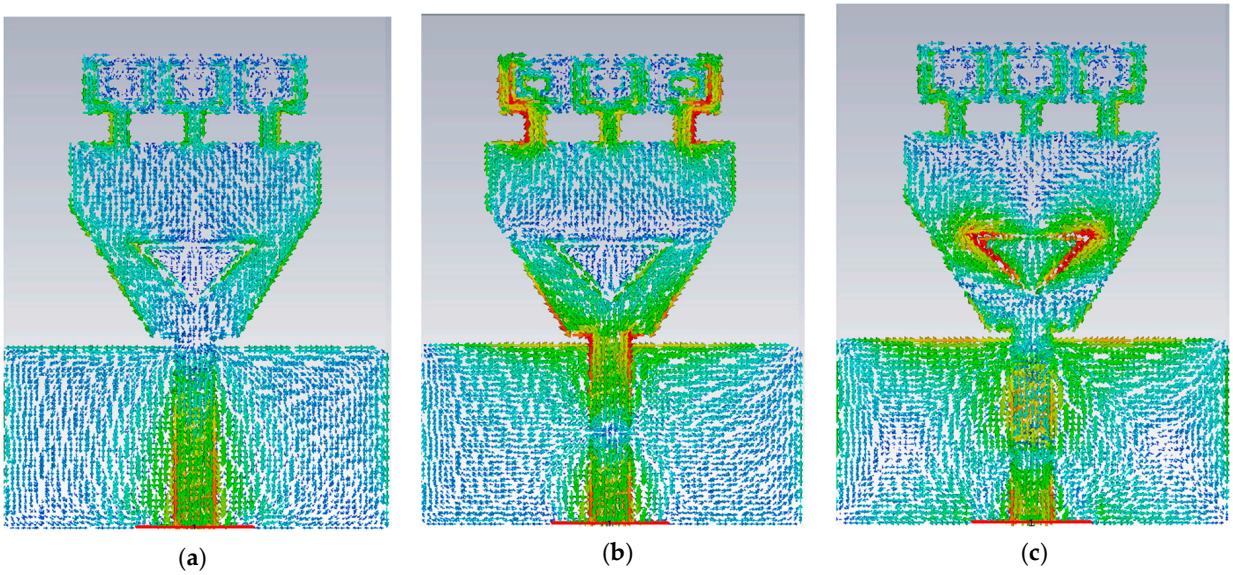

Figure 7. Surface current distributions of the proposed triple-band UWB antenna (**a**) 3.5 GHz (**b**) 6.1 GHz (**c**) 9.25 GHz.

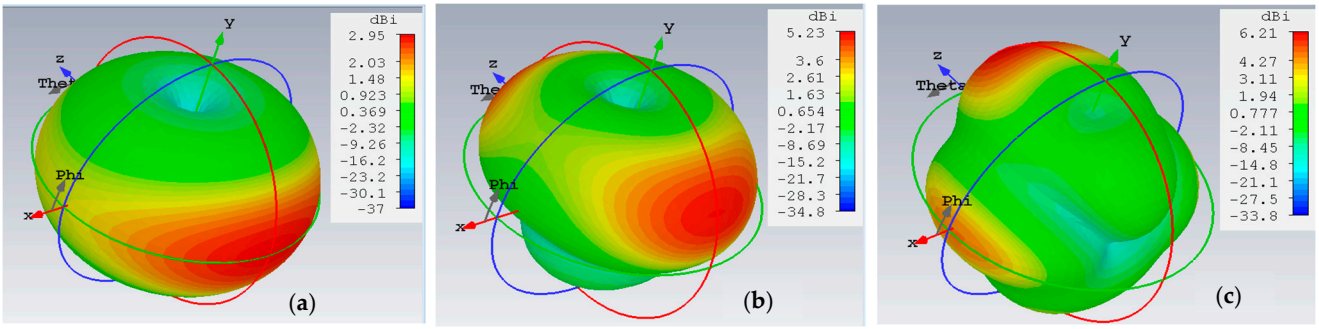

Figure 8. Simulated 3D RPs at (**a**) 3.5 GHz (**b**) 6.1 GHz (**c**) 9.25 GHz.

3. Parametric Study

In the parametric analysis, a comparative study of S-parameter performance has been carried out by varying the dimensions of triangular slot width (*S*) and SSRR slot width (*t*) of the radiating patch as illustrated in Figure 9a,b. From Figure 9a, it can be understood that one of the rejection band frequencies shown in Table 2 can be shifted by varying the dimension '*S*' on the main radiating patch. At *S* = 0.65 mm, 0.9 mm, and 1.15 mm, the corresponding higher rejection-band frequencies are tuned between 6.72–9.1 GHz, 6.77–8.7 GHz, and 6.73–8.5 GHz, respectively, although the lower rejection-band between 4.2–5.45 GHz remains the same in all cases. The higher operational band is also varied accordingly. The second analysis has been performed by varying the dimensions of parameter '*t*' and it can be seen in Figure 9b, that the middle operational band was shifted. At *t* = 0.4 mm, 0.5 mm, and 0.6 mm, the middle operational band is tuned between 5.4–6.5 GHz, 5.45–6.77 GHz, and 5.45–6.98 GHz respectively.

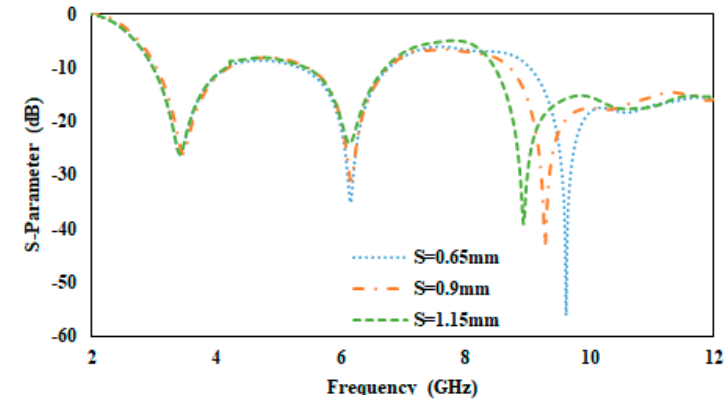

(**a**)

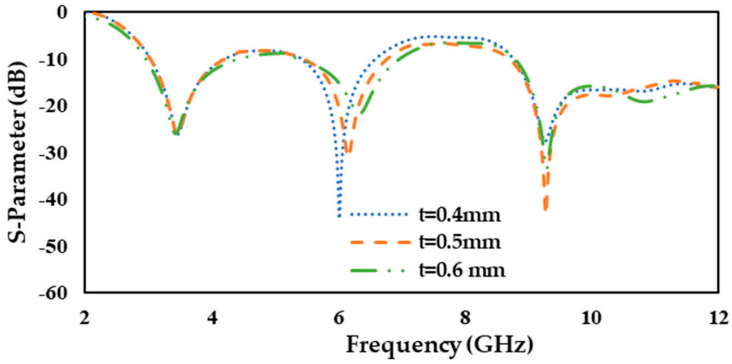

(**b**)

Figure 9. Simulated S-Parameter performance by varying (**a**) Triangular slot width (*S*) (**b**) SSRR slot width (*t*).

From Figure 9a,b, it can be seen that the higher operational band can be controlled by varying the parameter dimension '*S*', and the middle operational band can be controlled by changing the dimension of the parameter '*t*'. Table 3 shows the summarized value of the operational and rejection band by varying '*S*' and '*t*'.

Table 3. Operational and Rejection band coverage by varying parameters '*S*' and '*t*'.

Parameter	Operational Bands Coverage (GHz)	Rejection Bands Coverage (GHz)
S = 0.65 mm	3–4.2, 5.45–6.72, 9.1–12	4.2–5.45, 6.72–9.1
S = 0.9 mm	3–4.2, 5.45–6.77, 8.7–12	4.2–5.45, 6.77–8.7
S = 1.15 mm	3–4.2, 5.45–6.73, 8.5–12	4.2–5.45, 6.73–8.5
t = 0.4 mm	3–4.2, 5.4–6.5, 8.5–12	4.2–5.4, 6.5–8.5
t = 0.5 mm	3–4.2, 5.45–6.77, 8.7–12	4.2–5.45, 6.77–8.7
t = 0.6 mm	3–4.2, 5.45–6.98, 8.7–12	4.2–5.45, 6.98–8.7

4. Results and Discussion

Figure 10a,b shows the fabricated prototype (front and back view) of the proposed antenna and Figure 10c shows the antenna measurement setup arranged inside an anechoic chamber. The simulated results are obtained by using the commercial software CST-MWS which is based on the Finite Integration Technology (FIT). The reflection coefficient (S_{11}) measurements are performed by using a Rhode & Schwarz ZVL vector network analyzer (VNA). Figure 11a,b shows the simulated and measured return-loss and voltage standing wave ratio (VS.WR) [19] of the proposed dual-band notched antenna. The measured bandwidth covers the full UWB frequency range from 3 GHz to 12 GHz, except for the two notched bands of 4.17–5.33 GHz and 6.5–8.9 GHz. The first notched band covers some portion of the C-band, and the second notched band covers the downlink of the X-band satellite communication systems. The measured three operational frequency covers the range between 3–4.17 GHz, 5.33–6.5 GHz, and 8.9–12 GHz. The simulated result presented in Table 2 closely matches the measured result shown in Figure 11. It can be understood from Figure 11 that there is a slight shift between the simulated and measured results due to the variation in the loss tangent of the FR4 substrate. This frequency shift problem can be solved in the future by using a low-loss Rogers substrate.

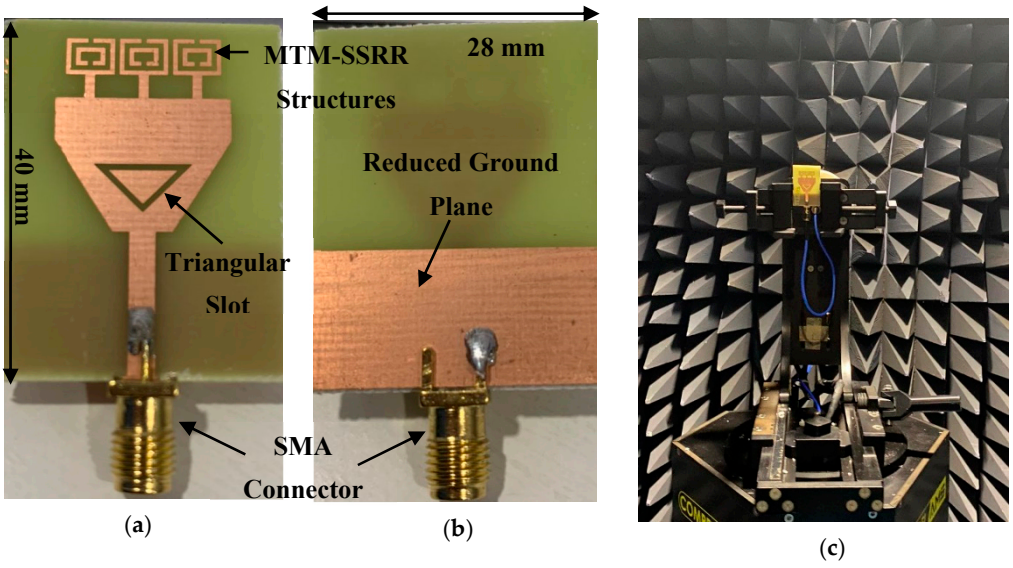

Figure 10. Fabricated Prototype of Proposed Antenna (**a**) Top-layer (**b**) Bottom-layer (**c**) Anechoic chamber measurement setup.

Figure 12a-c shows the simulated and measured RPs of the designed UWB antenna with dual-notch band characteristics and its fabricated prototype. Both E- (yz-plane) and

H-plane (xz-plane) RPs at 3.5 GHz, 6.1 GHz, and 9.25 GHz are demonstrated, respectively. It can be observed from the results that the H-plane RPs are close to omni-directional shape i.e., similar to the one exhibited by a typical monopole antenna, over the UWB antenna bandwidth except for the two notched bands. From Figure 12a, it can be realized that the antenna radiates in all directions with a maximum measured gain of ≈2.5 dBi at 0° angle in the E- & H-plane. Similarly, in Figure 12b, the proposed antenna at 6.1 GHz achieved a maximum measured gain of ≈5 dBi at 15° angle in the E- & H-plane. The proposed antenna achieved the highest gain at 9.25 GHz, i.e., close to ≈5.3 dBi at 30° angle in E- and at 300° in the H-plane as shown in Figure 12c. The simulated and measured gain at the complete operating bandwidth of the antenna are shown in Figure 13. It can be observed from the results that the simulated results are in good agreement with the measured results within the experimental errors.

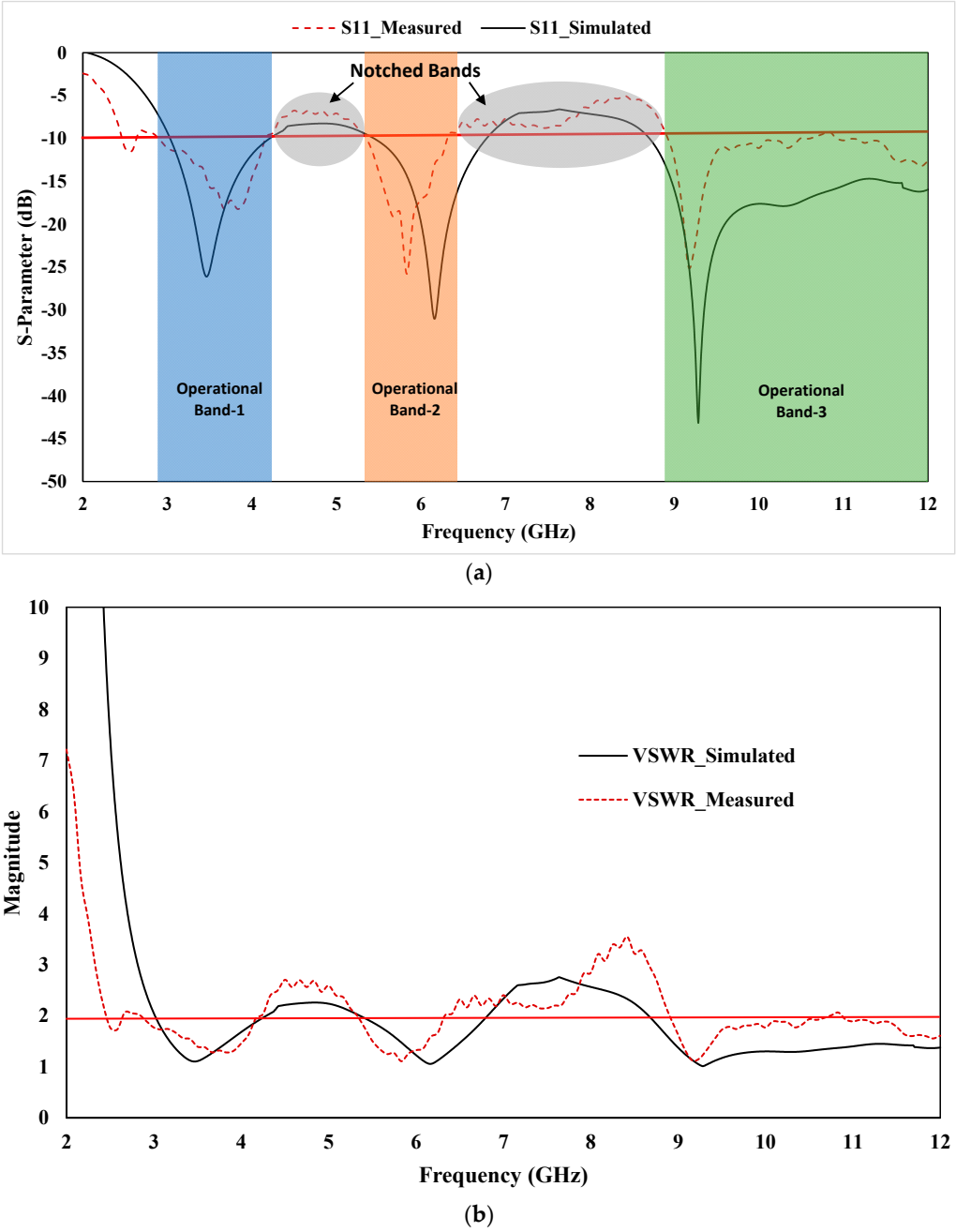

Figure 11. Simulated and measured S-parameter response of the proposed antenna (**a**) Return-loss and (**b**) VS.WR.

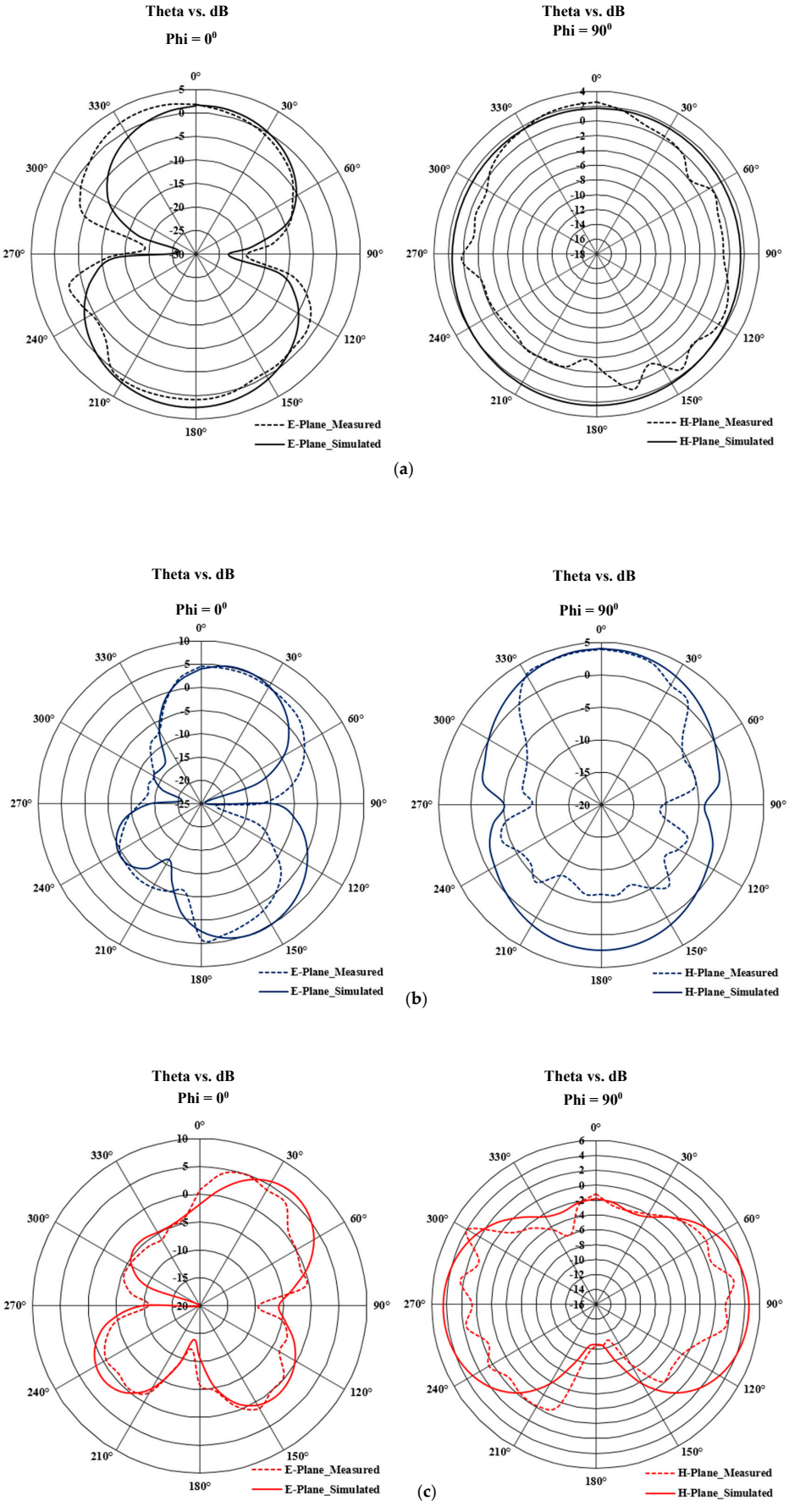

Figure 12. Simulated and measured E- & H-plane RP (**a**) 3.5 GHz (**b**) 6.1 GHz (**c**) 9.25 GHz.

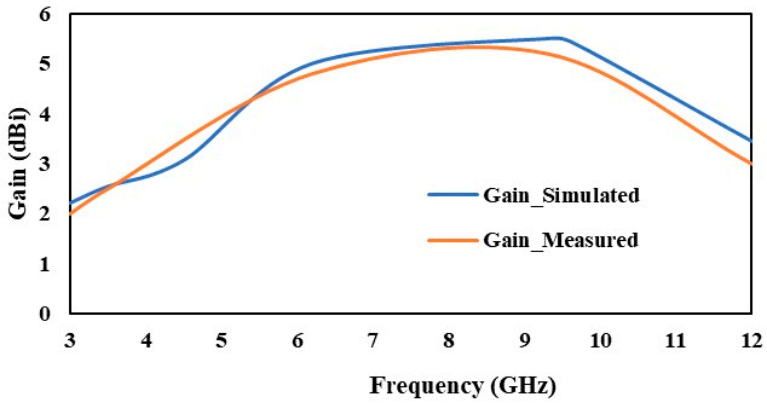

Figure 13. Gain vs. frequency graph of the proposed UWB antenna.

5. Comparative Study

Finally, Table 4 compares the proposed antenna from this work to the MTM-based antennas that have been previously reported in [12,18,29,31,32,35] in terms of size, substrate dielectric constant, number of notch-bands, controllability of the notch-band bandwidth and frequency, technique, the complexity of the design, and operational bandwidth. It can be observed from Table 4 that, out of all the antennas presented, nearly all of them are unable to control the notch-bandwidth and frequency. The antenna reported in [12,18] has a single notch-band with compact size and only the article [18] has demonstrated the feature of controlling only one notch-band bandwidth. The antennas described in [31,32] provide triple notch-bands based on the MTM technique, but the former lack the benefits of controllable notch-bandwidth and frequency, and the latter have the drawback of a complex design with the option of just one controllable notch-bandwidth and frequency, which is caused by the presence of a varactor diode. The antenna designs indicated in [29,35] offer a dual notch-band without notch-bandwidth and frequency controllable benefits; the former has a compact size, while the latter has a large size. Most of the antenna designs presented in Table 4 use high-end substrates. In summary, the proposed inverted triangular antenna has the features of low-cost, compact size, and simple design with the option of controllable bandwidth and frequency of the notch and operational band. The main contribution of this paper is that the antenna has features of controllable notch-bands that cover some portion of the C-band and downlink of the X-band satellite communication systems.

Table 4. Comparative study between the proposed antenna and existing MTM-based antennas.

Ref No./Year	Size (mm^3)	Substrate (ε_r)	No. of Notch Band	Coverage of Bands (GHz)	Controllable Notch-Bandwidth	Controllable Notch Frequency	Technique	Complexity	Operational Bandwidth (GHz)
[12]/2020	20.5 × 13.9 × 0.012	3.5	1	7.9–8.4	No	No	Complimentary-SRR (CSRR)	High	3.6–19.08
[18]/2020	16 × 25 × 1.52	2.17	1	5–6	Yes	Yes	EBG	Low	3.1–12.5
[29]/2021	25 × 35 × 1.6	4.3	2	3.11–4.01, 5.15–5.98	No	No	Open meander slitted EBG structure	Low	2.63–13
[31]/2018	36 × 34 × 1	2.65	3	3.97–4.48, 5.79–6.57, 7.30–7.60	Only one lower notch band controllable	Only one notch frequency controllable	Elliptical and circular ring resonators	High/Active elements are there	3.1–10.6
[32]/2021	20 × 26 × 1.52	2.17	3	3.4–3.95, 5.15–5.82, 7.25–7.75	No	No	EBG and SRR	High	3.1–11.8
[35]/2014	50 × 50 × 1.575	2.33	2	5.15–5.82, 6.2–6.9 GHz	No	No	SRR	Low	3.1–10
This work/2022	28 × 40 × 1.6	4.3	2	4.17–5.33, 6.5–8.9	Yes	Yes	SSRR and Triangular slot	Low	3–12

6. Conclusions

A compact and planar dual-notch band antenna with the dimensions of 28 mm × 40 mm printed on a low-cost FR4 substrate has been proposed for UWB systems. A dual-band rejection has been investigated by inserting three MTM-SSRRs and a triangular slot on the radiating patch. The measured results show that the fabricated antenna is appropriate for the UWB band operation between the frequency range of 3–12 GHz and a dual band-notched characteristic at 4.17–5.33 GHz and 6.5–8.9 GHz. The first notched-band cover some portion of the C-band and the second notched-band cover the downlink frequency range of the X-band satellite communication systems. Furthermore, omni-directional radiation pattern characteristics have been observed with a gain of ~2.5 dBi, ~5 dBi, and ~5.3 dBi at the center frequency of 3.5 GHz, 6.1 GHz, and 9.25 GHz, respectively. The tunability/controllability of the dual-notch band has been investigated by modifying the width of the triangular and the SSRR slots. The simulated and measured results of the proposed antenna show good agreement with each other, and it is envisioned that the proposed antenna will become an excellent candidate for the 5G mobile BSs, next-generation WiFi-6E IDAS, as well as C-band and X-band applications.

Author Contributions: A.K.V., B.A.K. coined the idea, led, supervised, and evaluated the entire project: edited the write-ups, designed, and simulated the proposed antennas. A.K.V., M.K.A.R., M.N.I. performed the experimental measurements. A.K.V. completed the initial draft of the paper; A.K.V., B.A.K., M.K.A.R., M.N.I., H.T.C. and M.F.b.M.A. then analyzed, evaluated, and edited the paper. All authors have read and agreed to the published version of the manuscript.

Funding: This research was funded by "Deanship of Scientific Research, Islamic University of Madinah, Madinah, Saudi Arabia, Grant Number 657".

Institutional Review Board Statement: Not applicable.

Informed Consent Statement: Not applicable.

Data Availability Statement: Not applicable.

Acknowledgments: The authors would like to acknowledge the funding from the Deanship of Scientific Research, Islamic University of Madinah, Madinah, Saudi Arabia, under the Research Grant No. 657.

Conflicts of Interest: The authors declare no conflict of interest.

References

1. Liaskos, C.; Mamatas, L.; Pourdamghani, A.; Tsioliaridou, A.; Ioannidis, S.; Pitsillides, A.; Schmid, S.; Akyildiz, I.F. Software-Defined Reconfigurable Intelligent Surfaces: From Theory to End-to-End Implementation. *Proc. IEEE* **2022**, 1–28. [CrossRef]
2. Rappaport, T.S.; Xing, Y.; Kanhere, O.; Ju, S.; Madanayake, A.; Mandal, S.; Alkhateeb, A.; Trichopoulos, G.C. Wireless Communications and Applications above 100 GHz: Opportunities and Challenges for 6G and beyond. *IEEE Access* **2019**, *7*, 78729–78757. [CrossRef]
3. America's 5G Future. Available online: https://www.fcc.gov/5G (accessed on 14 July 2022).
4. Shafique, K.; Khawaja, B.A.; Sabir, F.; Qazi, S.; Mustaqim, M. Internet of Things (IoT) for Next-Generation Smart Systems: A Review of Current Challenges, Future Trends and Prospects for Emerging 5G-IoT Scenarios. *IEEE Access* **2020**, *8*, 23022–23040. [CrossRef]
5. Vallappil, A.K.; Rahim, M.K.A.; Khawaja, B.A.; Murad, N.A.; Mustapha, M.G. Butler Matrix Based Beamforming Networks for Phased Array Antenna Systems: A Comprehensive Review and Future Directions for 5G Applications. *IEEE Access* **2020**, *9*, 3970–3987. [CrossRef]
6. Stefanini, L.; Rech, A.; Ramaccia, D.; Tomasin, S.; Toscano, A.; Moretto, F.; Bilotti, F. Multibeam Scanning Antenna System Based on Beamforming Metasurface for Fast 5G NR Initial Access. *IEEE Access* **2022**, *10*, 65982–65995. [CrossRef]
7. Razzaqi, A.A.; Khawaja, B.A.; Ramzan, M.; Zafar, M.J.; Nasir, S.A.; Mustaqim, M.; Tarar, M.A.; Tauqeer, T. A triple-band antenna array for next-generation wireless and satellite-based applications. *Int. J. Microw. Wirel. Technol.* **2014**, *8*, 71–80. [CrossRef]
8. David, R.M.; AW, M.S.; Ali, T.; Kumar, P. A Multiband Antenna Stacked with Novel Metamaterial SCSRR and CSSRR for WiMAX/WLAN Applications. *Micromachines* **2021**, *12*, 113. [CrossRef]
9. Khawaja, B.A.; Tarar, M.A.; Tauqeer, T.; Amir, F.; Mustaqim, M. A 1 × 2 Triple Band Printed Antenna Array for Use in Next Generation Flying Ad-Hoc Networks (FANETs). *Microw. Opt. Technol. Lett.* **2016**, *58*, 606–610. [CrossRef]
10. Ali, Q.; Shahzad, W.; Ahmad, I.; Safiq, S.; Bin, X.; Abbas, S.M.; Sun, H. Recent Developments and Challenges on Beam Steering Characteristics of Reconfigurable Transmitarray Antennas. *Electronics* **2022**, *11*, 587. [CrossRef]

11. Modak, S.; Khan, T. A slotted UWB-MIMO antenna with quadruple band-notch characteristics using mushroom EBG structure. *AEU Int. J. Electron. Commun.* **2021**, *134*, 153673. [CrossRef]
12. Zou, Q.; Jiang, S. A compact flexible fractal ultra-wideband antenna with band notch characteristic. *Microw. Opt. Technol. Lett.* **2020**, *63*, 895–901. [CrossRef]
13. Nikolaou, S.; Abbasi, M.A.B. Design and Development of a Compact UWB Monopole Antenna with Easily-Controllable Return Loss. *IEEE Trans. Antennas Propag.* **2017**, *65*, 2063–2067. [CrossRef]
14. Tian, M.; Yan, N.; Luo, Y.; Ma, K. A Low-Cost High-Gain Filtering Patch Antenna Using SISL Technology for 5G Application. *IEEE Antennas Wirel. Propag. Lett.* **2021**, *20*, 2270–2274. [CrossRef]
15. Cai, C.-A.; Kai, K.-Y.; Liao, W.-J. A WLAN/WiFi-6E MIMO Antenna Design for Handset Devices. In Proceedings of the 2021 International Symposium on Antennas and Propagation (ISAP), Taipei, Taiwan, 19–22 October 2021. [CrossRef]
16. Ullah, R.; Ullah, S.; Faisal, F.; Ullah, R.; Ben Mabrouk, I.; Al Hasan, M.J.; Kamal, B. A novel multi-band and multi-generation (2G, 3G, 4G, and 5G) 9-elements MIMO antenna system for 5G smartphone applications. *Wirel. Netw.* **2021**, *27*, 4825–4837. [CrossRef]
17. El-Khamy, S.E.; Zaki, A.; Hamdy, S.; El-Khouly, A. A new fractal-like tree structure of circular patch antennas for UWB and 5G multi-band applications. *Microw. Opt. Technol. Lett.* **2017**, *59*, 2168–2174. [CrossRef]
18. Abbas, A.; Hussain, N.; Jeong, M.-J.; Park, J.; Shin, K.S.; Kim, T.; Kim, N. A Rectangular Notch-Band UWB Antenna with Controllable Notched Bandwidth and Centre Frequency. *Sensors* **2020**, *20*, 777. [CrossRef]
19. Balanis, C.A. *Antenna Theory: Analysis and Design*, 4th ed.; Wiley: Hoboken, NJ, USA, 2016.
20. Vallappil, A.K.; Khawaja, B.A.; Rahim, M.K.A.; Iqbal, M.N.; Chattha, H.T. Metamaterial-Inspired Electrically Compact Triangular Antennas Loaded with CSRR and 3 × 3 Cross-Slots for 5G Indoor Distributed Antenna Systems. *Micromachines* **2022**, *13*, 198. [CrossRef]
21. Cicchetti, R.; Miozzi, E.; Testa, O. Wideband and UWB Antennas for Wireless Applications: A Comprehensive Review. *Int. J. Antennas Propag.* **2017**, *2017*, 1–45. [CrossRef]
22. Shafique, K.; Mustaqim, M.; Khan, B.M.; Khawaja, B. A Thin and Flexible Ultra Wideband Antenna for Wireless Body Area Networks with Reduced Ground Plane Effect. In Proceedings of the 2015 IEEE Conference on Emerging Technologies (ICET), Peshawar, Pakistan, 19–20 December 2015.
23. Kumar, O.P.; Kumar, P.; Ali, T.; Kumar, P.; Vincent, S. Ultrawideband Antennas: Growth and Evolution. *Micromachines* **2022**, *13*, 60. [CrossRef]
24. Mustaqim, M.; Khawaja, B.A.; Chattha, H.T.; Shafique, K.; Zafar, M.J.; Jamil, M. Ultra Wideband Antenna for Wearable Internet of Things Devices and Wireless Body Area Network Applications. *Int. J. Numer. Model. Electron. Netw. Devices Fields* **2019**, *32*, e2590. [CrossRef]
25. Ganesan, I.; Iyampalam, P. A Review of Ultra-Wideband Fractal Antennas. In Proceedings of the 2018 Second International Conference on Inventive Communication and Computational Technologies (ICICCT), Coimbatore, India, 20–21 April 2018; pp. 1408–1412. [CrossRef]
26. Reddy, A.P.; Muthusamy, P. A Review on UWB Metamaterial Antenna. In *Innovations in Electronics and Communication Engineering. Lecture Notes in Networks and Systems*; Saini, H.S., Singh, R.K., Tariq Beg, M., Sahambi, J.S., Eds.; Springer: Berlin, Germany, 2020; Volume 107. [CrossRef]
27. Shome, P.P.; Khan, T.; Koul, S.K.; Antar, Y.M. Two Decades of UWB Filter Technology: Advances and Emerging Challenges in the Design of UWB Bandpass Filters. *IEEE Microw. Mag.* **2021**, *22*, 32–51. [CrossRef]
28. Rahman, M.; Khan, W.T.; Imran, M. Penta-notched UWB antenna with sharp frequency edge selectivity using combination of SRR, CSRR, and DGS. *AEU Int. J. Electron. Commun.* **2018**, *93*, 116–122. [CrossRef]
29. Alizadeh, F.; Ghobadi, C.; Nourinia, J.; Abdi, H.; Mohammadi, B. UWB dual-notched planar antenna by utilizing compact open meander slitted EBG structure. *AEU Int. J. Electron. Commun.* **2021**, *136*, 153715. [CrossRef]
30. Kumar, G.; Singh, D.; Kumar, R. A planar CPW fed UWB antenna with dual rectangular notch band characteristics incorporating U-slot, SRRs, and EBGs. *Int. J. RF Microw. Comput. Eng.* **2021**, *31*, e22676. [CrossRef]
31. Rahman, S.U.; Cao, Q.; Li, Y.; Gil, I.; Yi, W. Design of tri-notched UWB antenna based on elliptical and circular ring resonators. *Int. J. RF Microw. Comput. Eng.* **2018**, *29*, e21648. [CrossRef]
32. Abbas, A.; Hussain, N.; Lee, J.; Park, S.G.; Kim, N. Triple Rectangular Notch UWB Antenna Using EBG and SRR. *IEEE Access* **2020**, *9*, 2508–2515. [CrossRef]
33. Chakraborty, M.; Pal, S.; Chattoraj, N. Quad notch UWB antenna using combination of slots and split-ring resonator. *Int. J. RF Microw. Comput. Eng.* **2019**, *30*, e22086. [CrossRef]
34. Veselago, V.; Braginsky, L.; Shklover, V.; Hafner, C. Negative Refractive Index Materials. *J. Comput. Theor. Nanosci.* **2006**, *3*, 189–218. [CrossRef]
35. Siddiqui, J.Y.; Saha, C.; Antar, Y.M.M. Compact Dual-SRR-Loaded UWB Monopole Antenna with Dual Frequency and Wideband Notch Characteristics. *IEEE Antennas Wirel. Propag. Lett.* **2014**, *14*, 100–103. [CrossRef]